ACS Partner Journal
PRECISION CHEMISTRY

pubs.acs.org/PrecisionChem
Article

Synthesis, Structures, and Chiroptical Properties of NBN-Doped Helicenes with Boron Atoms in the Inner Rims

Weiwen Zhuang,† Yujian Liu,† Ziqi Deng, Yu Guo, Philip C. Y. Chow, David Lee Phillips, Wei Jiang, Zhaohui Wang,* and Junzhi Liu*

Cite This: *Precis. Chem.* 2024, 2, 28−39
Read Online
ACCESS | Metrics & More | Article Recommendations | Supporting Information

ABSTRACT: The precise synthesis of helicenes with topologically defined length and specific heteroatomic perturbation in the screw-like conjugated skeletons plays an emerging role in the manipulation of chiral materials. Facile, selective, and programmable routes to helicenes or heterohelicenes are highly desirable yet challenging for structure−chiroptical property relationship studies. Herein, we report the synthesis and characterization of NBN-doped helicenes with boron atoms in the inner rims, enabled by the highly regioselective one-pot borylation of rationally designed precursors with, namely, fold-in or pan-out manner. The incorporation of nonbonded boron and nitrogen atoms resulted in narrow-band emission and improved optical properties for the single-stranded carbon helix. In addition, numbers and arrangement modes of fused six-membered rings have distinct effects on configurational stability and chiroptical properties, revealing that **BN-[6]H** with strong circular dichroism is a promising candidate for chiral sensors. The combination of experimental and theoretical studies on these helical structures might provide insights into the design of helically chiral small-molecule-based sensors or emitters.

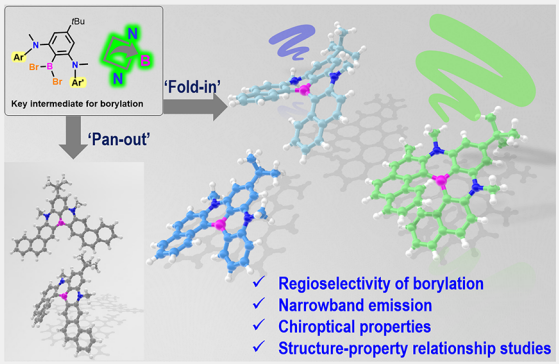

KEYWORDS: *Nitrogen−boron, Helicenes, Borylation, Chiroptical properties, Narrow-band emission*

INTRODUCTION

Helicenes, which are an intriguing class of aesthetically appealing polycyclic aromatic hydrocarbons (PAHs) consisting of consecutive angular-fused aromatic rings, have attracted considerable attention since the pioneering work of Meisenheimer and Witte in 1903.[1−6] Their helically chiral topologies lead to unique packing in the solid state or molecular dynamics in solution, and endow the materials with fascinating chiroptical properties for applications in advanced optoelectronic devices, such as chiroptical sensors,[7,8] spin filters,[9,10] and photoswitches.[11] However, the flexible backbones of helicenes enhance structural relaxation in the excited states, resulting in broadened emission peaks. Furthermore, intersystem crossing in helicenes usually decreases the quantum yield of fluorescence (Φ_F), which further limits their applications of these materials in practical organic photodevices.[12−17]

Modifying the periphery of helicenes with grafted donor/acceptor groups or transition metals is a popular strategy to improve their novel chiral photophysical properties, e.g., circular dichroism (CD), Raman optical activity (ROA), and circularly polarized luminescence (CPL).[18,19] However, "spine surgery" of their highly twisted backbones provides more opportunities for enhancing the helicities and tuning the chiroptical properties of these compounds. This approach is characterized by (i) angular or linear fusion of more benzene rings (higher or expanded helicenes),[20−23] (ii) integration of multiple helicities,[24−26] (iii) the introduction of nonbenzenoid subunits,[27−31] and (iv) the incorporation of main group elements (heterohelicenes).[5]

The simultaneous introduction of boron (B) and nitrogen (N) atoms into PAHs epitomizes the synergistic benefits from the electron accepting and donating natures of boron and nitrogen, respectively, to tailor their photophysical and electrochemical properties.[32−34] Despite the significant progress in exploring the chemical space of heteroarenes featuring azaborine rings,[35−38] the bottom-up synthesis of BN-doped heterohelicenes through rational design is relatively rare owing to synthetic challenges.

The replacement of C═C units with isoelectronic B═N units is a recognized approach to construct structurally unique heterohelicenes, where N-directed borylation facilitates the formation of helical skeletons with boron atoms in the outer rims (Figure 1a).[39−42] In 2012, Hatakeyama, Nakamura and coworkers synthesized azaboradibenzo[6]helicene and investigated the carrier inversion behavior of the racemate and the single enantiomer (Figure 1a, top).[39] In 2022, Nowak-Król,

Received: September 28, 2023
Revised: November 13, 2023
Accepted: November 21, 2023
Published: December 18, 2023

https://doi.org/10.1021/prechem.3c00097
Precis. Chem. 2024, 2, 28−39

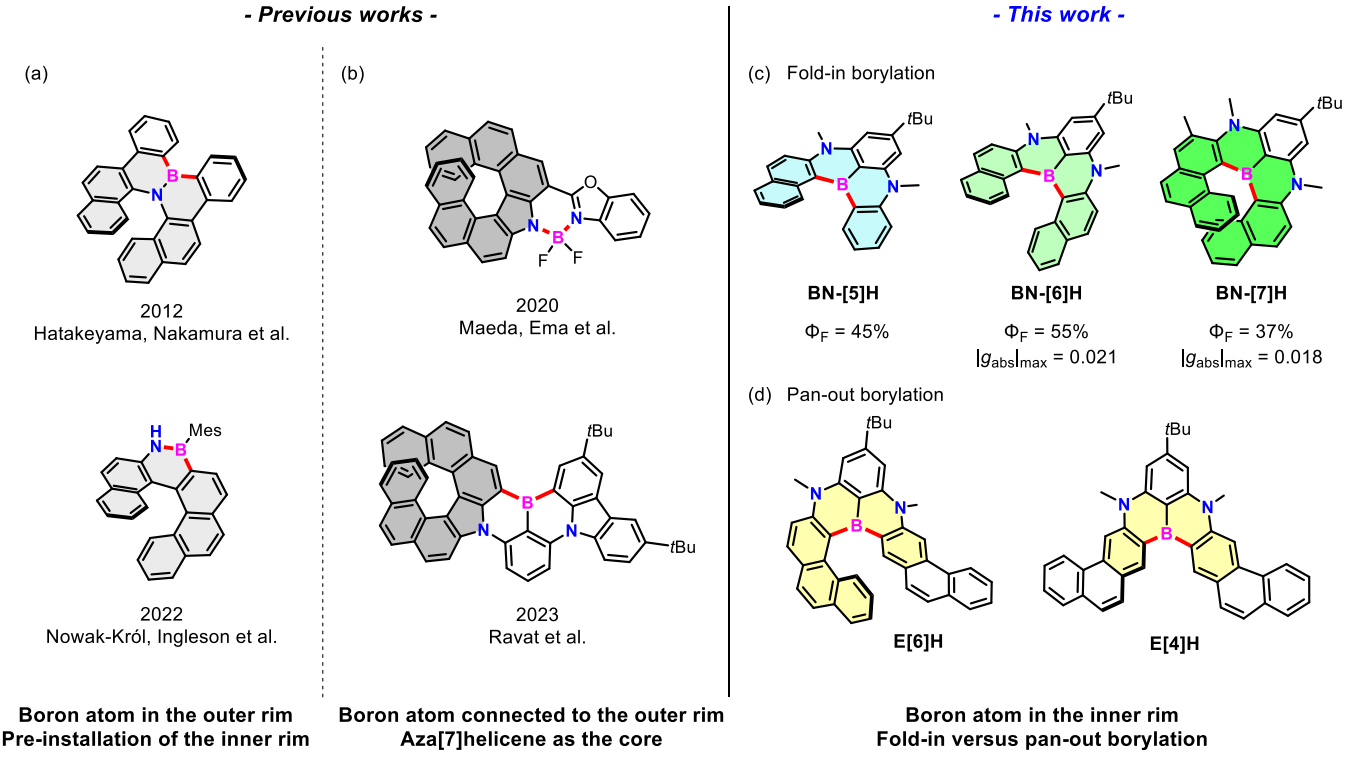

Figure 1. (a) BN-doped [6]helicenes with boron atoms in the outer rims; (b) NBN-doped helicenes based on aza[7]helicene with boron atoms connected to the outer rims; (c, d) NBN-doped helicenes with boron atoms in the inner rims in this work via one-pot borylation with a fold-in or pan-out manner.

Ingleson and co-workers exploited the acid-enhanced reactivity toward N-directed C−H borylation and synthesized BN-[6]helicene (Figure 1a, bottom).[40] In spite of the elegant examples of 1,2-azaborine-based helicenes, 1,4-azaborine-embedded helicenes remain elusive. Only an expanded helicene[23] and a few multiple helicenes[43−46] based on 5,9-diphenyl-5,9-dihydro-5,9-diaza-13*b*-boranaphtho[3,2,1-de]-anthracene (DABNA)[35] have been reported very recently. On the other hand, the formation of aza[7]helicene is an efficient alternative approach toward BN-doped heterohelicenes, where the boron atoms are connected to the outer rims via B−N or B−C bonds (Figure 1b).[47,48] The fusion of helically chiral auxiliaries into cores (BODIPY in Figure 1b, top;[47] DABNA in Figure 1b, bottom[48]) with exceptional photophysical properties leads to new synthetic paths to generate chiral materials. The scarcity of configurationally stable analogs of carbo[n]helicenes ($n > 4$) featuring 1,4-azaborines with boron atoms in the inner rims might be ascribed to the high torsional strain of helicenes and the Lewis acidity of triarylboranes.[49−51]

Herein, we report a one-pot borylation approach with, namely, fold-in selectivity for the modular synthesis of unprecedented NBN-doped benzo[n]helicenes (**BN-[*n*]H**, n = 5−7, Figure 1c) consisting of two 1,4-azaborines with a shared boron atom in the inner rim, which provides a suitable platform for the structure−property relationship studies. Moreover, a distinct pan-out borylation reaction affording π-extended helicenes (**E[6]H** and **E[4]H**) was observed, when a linear precursor with two phenanthrene moieties was applied (Figure 1d). The fold-in approach with excellent regioselectivity at the naphthalene moieties is a complementary method for the construction of BN-embedded helicenes beyond the chemical curiosity.[17,39−42] The pan-out borylation reaction highlights the innate ability of steric hindrance to invert the intrinsic selectivity during intramolecular electrophilic C−H borylation. Because of the introduction of a nonbonded N/B/N-unit, the resultant NBN-helicenes gave rise to narrow emission peaks with similar full width at half-maximum (fwhm) values ($fwhm_{BN\text{-}[5]H}$ = 25 nm; $fwhm_{BN\text{-}[6]H}$ = 23 nm; $fwhm_{BN\text{-}[7]H}$ = 43 nm) and improved photoluminescence efficiency ($\Phi_{BN\text{-}[5]H}$ = 45%; $\Phi_{BN\text{-}[6]H}$ = 55%; $\Phi_{BN\text{-}[7]H}$ = 37%) compared with the corresponding pristine carbohelicenes ($\Phi_{[5]H}$ = 4%; $\Phi_{[6]H}$ = 4%; $\Phi_{[7]H}$ = 2%[12−17]). Although the longer C−B bonds in the inner rims induced lower racemization barriers, the enantiomers of configurationally stable **BN-[6]H** and **BN-[7]H** were successfully separated by chiral high-performance liquid chromatography (HPLC), exhibiting strong circular dichroism with maximum absorption dissymmetry factors (g_{abs}) of 0.021 and 0.018 for **BN-[6]H** and **BN-[7]H**, respectively (Figure 7c). Moreover, as a naphthalene-extended analogue of **BN-[6]H**, **E[6]H** has a much lower configurational stability. The work reported herein demonstrated the excellent potential of the fold-in and pan-out synthetic strategies for bottom-up fabrication of heteroatom-doped helicenes as promising chiroptical materials.

RESULTS AND DISCUSSION

Design and Synthesis

Prized for their high stability, sterically protected triarylboranes are sought-after motifs in numerous syntheses of B-doped PAHs. However, the possible stitching approach toward NBN-doped helicenes is impeded by the scarcity of reliable synthesis and postsynthetic transformations of sterically hindered triarylborane intermediates (**Int. A**) with secondary amine scaffolds (Figure 2a).[52−54] To address the stability/reactivity challenge, we applied the versatile one-pot borylation reaction of precursors with preinstallation of nitrogen-bridged outer rims,

https://doi.org/10.1021/prechem.3c00097
Precis. Chem. 2024, 2, 28−39

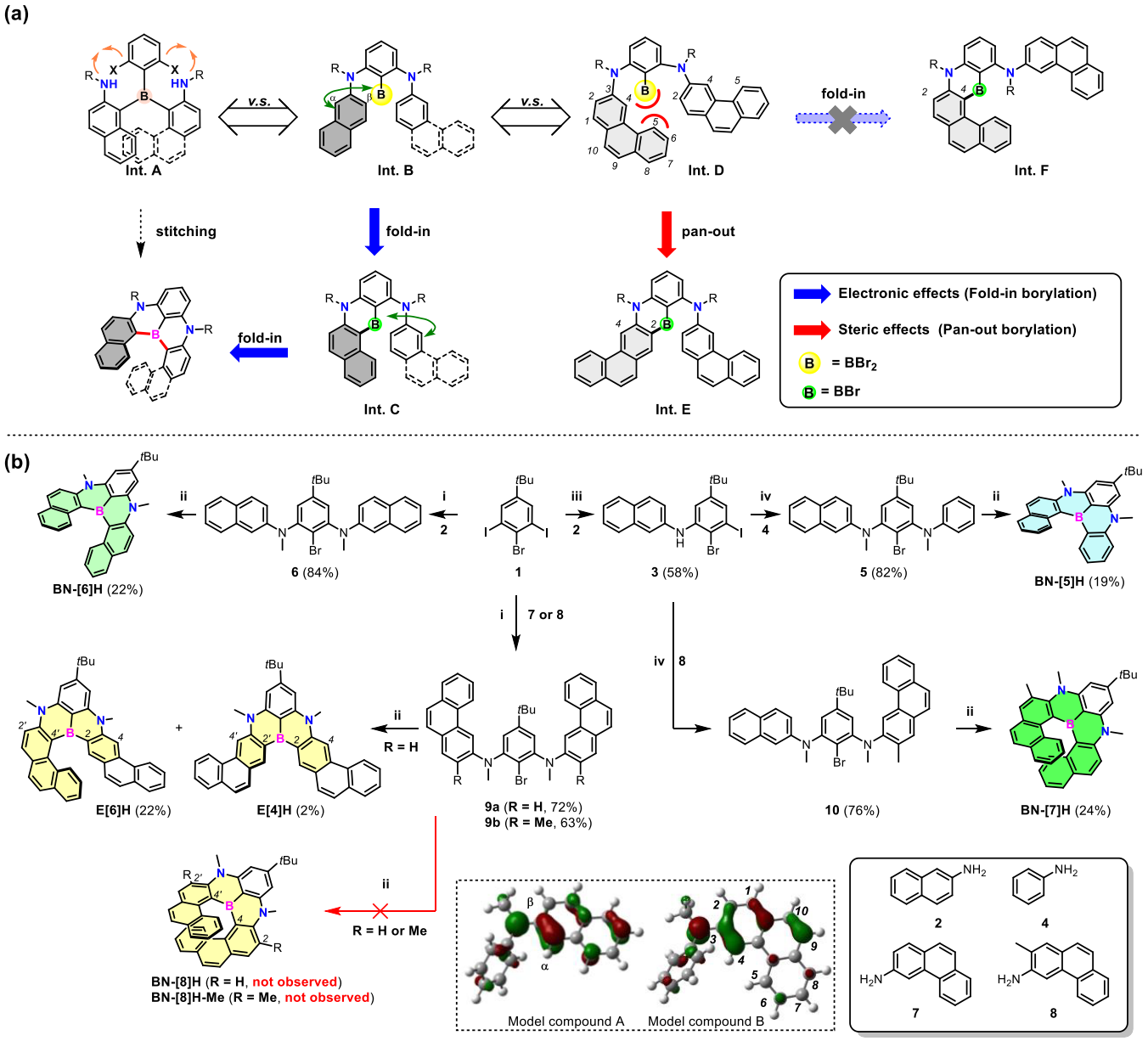

Figure 2. (a) One-pot borylation with fold-in or pan-out selectivity toward NBN-doped helicenes. (b) Synthesis of NBN-doped helicenes. HOMOs of model compounds A and B are shown in the dashed box. Reagents and conditions: (i) (1) $Pd_2(dba)_3$, dppf, *t*-BuONa, toluene, 90 °C; (2) NaH, MeI, THF, rt to 65 °C. (ii) (1) *n*-BuLi, *o*-xylene, rt to 50 °C; (2) BBr_3, 0 °C to rt. (3) Hunig's base, 0 to 130 °C. (iii) $Pd_2(dba)_3$, dppf, *t*-BuONa, toluene, 60 °C. (iv) (1) $Pd_2(dba)_3$, dppf, *t*-BuONa, toluene, 100 °C; (2) NaH, MeI, THF, rt to 65 °C. *t*-BuONa, sodium *tert*-butoxide; $Pd_2(dba)_3$, tris(dibenzylideneacetone)dipalladium(0); dppf, 1,1′-bis(diphenylphosphino)ferrocene; *n*-BuLi, *n*-butyllithium.

introducing borom atoms in the inner helical rims, which involves selective C−H borylation at the α-positions of naphthalene moieties of dibromo(aryl)borane intermediates (**Int. B**) or dibromo(diaryl)borane intermediates (**Int. C**) (Figure 2a). Considering the possible isomers, borylation with excellent regioselectivity is highly desirable for the construction of NBN-doped benzo[*n*]helicenes, which could be regarded as a "fold-in" strategy.[55] When two phenanthrene units are present in **Int. D** (Figure 2a), due to the steric repulsion between the BBr_2 group and the hydrogen atom at position 5 of phenanthrene, the first Friedel−Crafts borylation of **Int. D** might favor position 2 to afford **Int. E** in a "pan-out" manner, while the "fold-in" borylation at more electron-rich position 4 affording **Int. F** is less accessible. The residual B−Br of **Int. E** is less bulky than the BBr_2 of **Int. D**; thus, the second electrophilic C−H borylation might be furnished at position 4. The lithiation-borylation sequence of bromoarenes is a feasible synthetic process to install boron atoms at specific sites, which is also suitable to prepare **Int. B** and **Int. D**. To simplify the regioselectivity of the annulation step, methyl groups, which are inert toward metal-free electrophilic C−H borylation, are introduced to the nitrogen atoms of linear triaryldiamine precursors. Fortunately, nitrogen-attached methyl groups are compatible with BBr_3 during the fold-in or pan-out closure of helical backbones, despite BBr_3 being one of the most popular reagents utilized in demethylation reactions.

To verify the hypothesis related to fold-in selectivity in the one-pot borylation reaction, the unsymmetric precursor **5** with only one naphthalene moiety was first prepared and subjected to the lithiation-borylation-annulation sequence (Figure 2b). With

https://doi.org/10.1021/prechem.3c00097
Precis. Chem. 2024, 2, 28−39

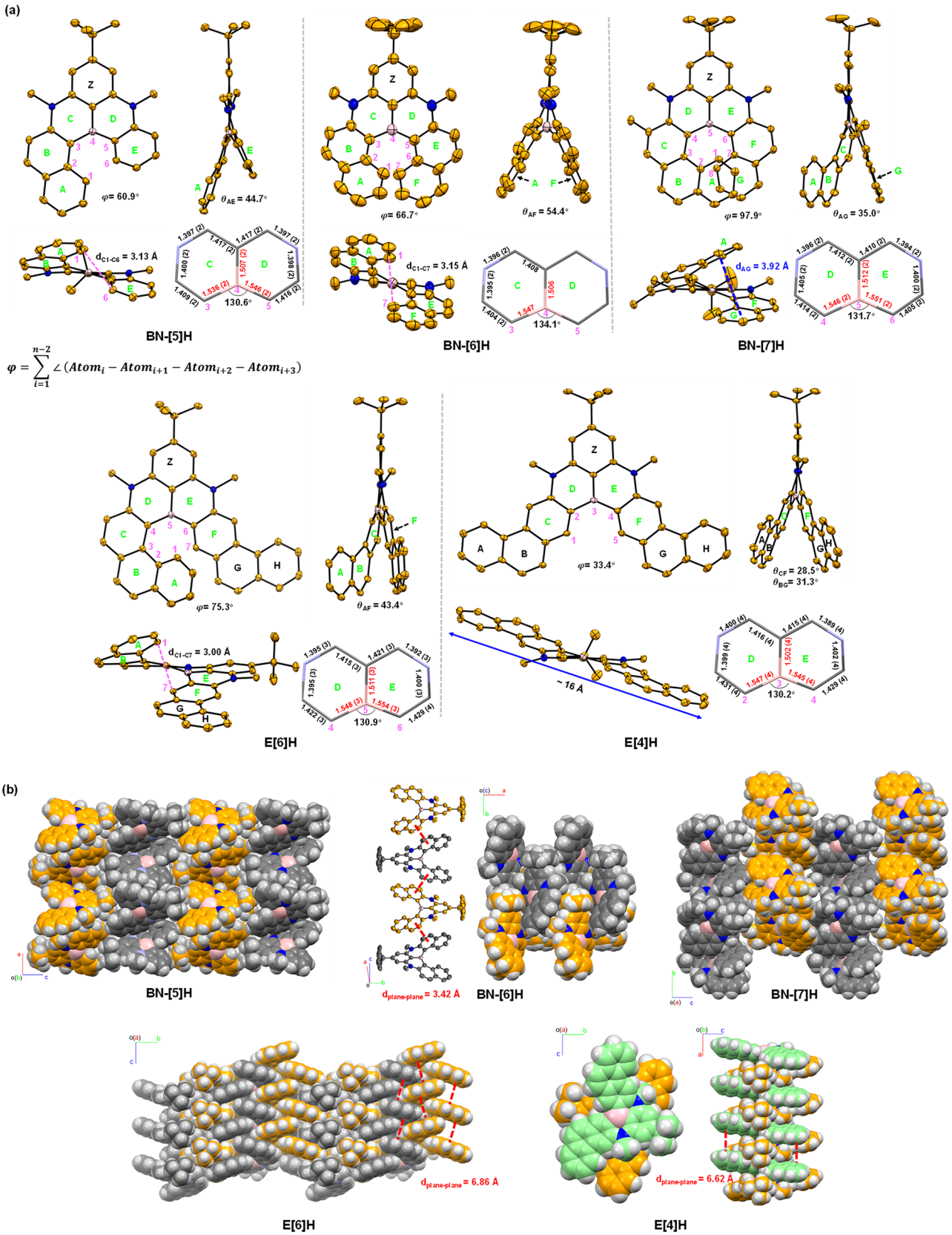

$$\varphi = \sum_{i=1}^{n-2} \angle(Atom_i - Atom_{i+1} - Atom_{i+2} - Atom_{i+3})$$

Figure 3. (a) Structures of NBN-doped helicenes. Thermal ellipsoids are shown at 50% probability; only (*P*)-enantiomers are shown, and hydrogen atoms are omitted for clarity. (b) Molecular packing in the crystals of NBN-doped helicenes. Carbon atoms of (*P*)-enantiomers are colored in orange and light green, and carbon atoms of (*M*)-enantiomers are colored in gray.

commercially available aniline derivatives in hand, the synthesis of **5** was started with selective one-fold palladium-catalyzed amination of **1** under a mild reaction condition using **2** as the limiting reagent, affording intermediate **3** in 58% yield. Coupling

https://doi.org/10.1021/prechem.3c00097
Precis. Chem. 2024, 2, 28−39

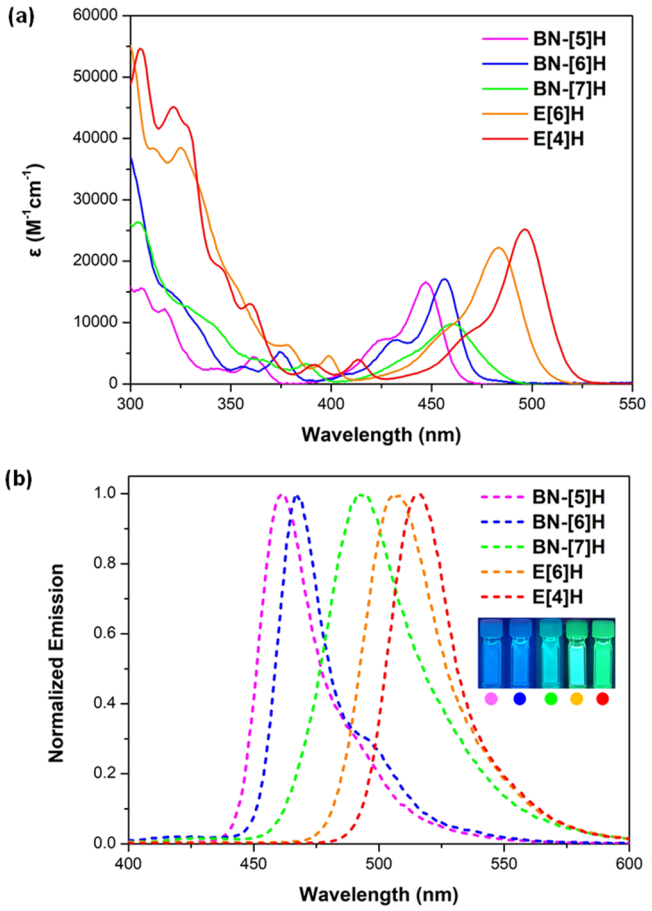

Figure 4. (a) UV−vis spectra and (b) normalized emission spectra of NBN-doped helicenes in toluene (~1×10^{-5} M). Inset: Photograph of the toluene solutions under UV light (365 nm).

of the residual iodine with aniline and the subsequent methylation with sodium hydride and iodomethane (NaH/MeI) provided **5** in 82% yield, which afforded **BN-[5]H** in 19% yield via one-pot borylation. After the lithium-halogen exchange, the addition of BBr_3 afforded a dibromo(aryl)borane intermediate, and then Hunig's base (*N*,*N*-diisopropylethylamine, DIPEA) promoted the formation of two additional B−C bonds at an elevated temperature (130 °C). Notably, absolute regioselectivity at a more electron-rich position (α-position of the naphthalene subunit) was observed.[56] Following the same strategy, symmetric precursor **6** with two naphthalene moieties was easily obtained by changing the limiting reagent from **2** to **1** during C−N coupling. The predominant bora-Friedel−Crafts reaction at the α-position of both naphthalene subunits afforded the fully fused skeleton of **BN-[6]H** in 22% yield, demonstrating the versality of the fold-in selectivity (Figure S3). As shown in the highest occupied molecular orbital (HOMO) distribution of model compound A (dashed box in Figure 2b), the β-position of naphthalene was electronically deactivated toward electrophilic borylation.

In light of these promising results, we examined the competitive interplay between steric hindrance, which favored a spatially more accessible site (position 2 of phenanthrene), and electronic effects, which steered the electrophilic borylation to a more electron rich site (position 4 of phenanthrene), as elucidated by the HOMO of model compound B (dashed box in Figure 2b). We found that subjecting **9a** to one-pot borylation condition led to **E[6]H** and **E[4]H** in a total yield of 24%, with a ratio of 11:1, while the fully fold-in analogue **BN-[8]H** was not observed. To further validate the pan-out trend in the first C−H borylation at position 2 of the phenanthrene moiety, precursor **9b** was synthesized and applied. As expected, no cyclized products were obtained, and even harsh conditions could not

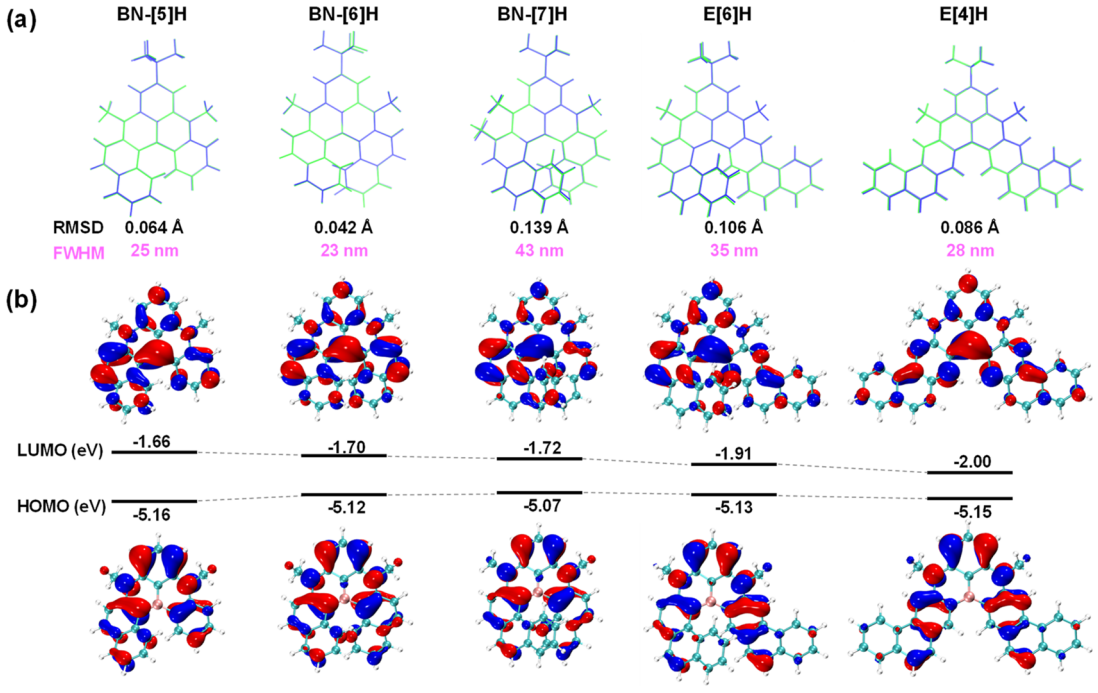

Figure 5. (a) Comparison of the S_0 (blue) and S_1 (green) geometries calculated at the (TD)B3LYP/6-31G(d) level. (b) Molecular orbitals calculated at the B3LYP-D3BJ/Def2-TZVP (solvent toluene, PCM model) level; *tert*-butyl groups and methyl group at the phenanthrene unit of **BN-[7]H** are reduced to hydrogen atoms for simplicity.

https://doi.org/10.1021/prechem.3c00097
Precis. Chem. 2024, 2, 28−39

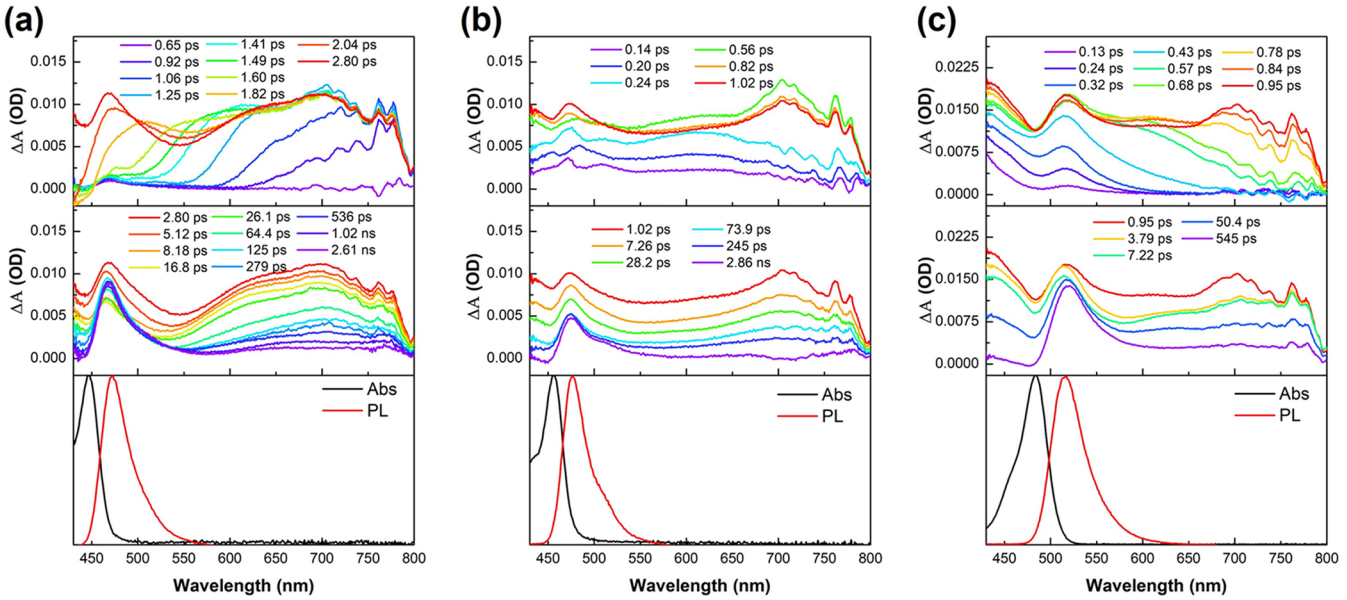

Figure 6. Femtosecond transient absorption spectra (top for early spectral conversion and middle for the late-time process) and normalized steady-state absorption/emission spectra (bottom) in dichloromethane of (a) **BN-[5]H**, (b) **BN-[6]H**, and (c) **E[6]H**.

Table 1. Summary of Optical and Electrochemical Properties of NBN-Doped Helicenes

sample	λ^{abs} (nm)[a]	λ_{max}^{em} (nm)[a]	$\upsilon_a - \upsilon_f$ (cm^{-1})[a]	fwhm (nm)[a]	RMSD (Å)[b]	PLQY (%)[a]	t (ns)[a]	E_{HOMO} (eV)[c]	E_{gap}^{opt} (eV)[d]	$\Delta E_{cal\text{-}H/L}$ (eV)[e]
BN-[5]H	447	461	679	25	0.064	45	6.5	−5.41	2.74	3.50
BN-[6]H	456	467	516	23	0.042	55	5.3	−5.43	2.69	3.42
BN-[7]H	460	494	1496	43	0.139	37	5.0	−5.39	2.61	3.35
E[6]H	483	507	980	35	0.106	49	6.0	−5.38	2.51	3.22
E[4]H	496	516	516	28	0.086	47	5.1	−5.43	2.45	3.15

[a]Measured in a toluene solution (~1 × 10^{-5} M) and determined using the absolute quantum yield method. [b]Calculated at the (TD)B3LYP/6-31G(d) level. [c]Estimated by the onset of the oxidation peaks in dichloromethane and calculated according to $E_{HOMO} = -(4.8 + E_{onset}^{ox})$ eV. [d]Estimated by the intersection of absorption and emission band. [e]Calculated at the B3LYP-D3BJ/Def2-TZVP (solvent toluene, PCM model) level.

induce the formation of B−C bonds to generate **BN-[8]H-Me** (Supporting Information).

Finally, we merged precursors **6** and **9b** into precursor **10**, containing naphthalene and methyl-blocked phenanthrene, to determine whether the fold-in selectivity was spatially and electronically accessible. To our delight, rationally designed **10** circumvented the issue of the contrast steering effect of sterics and electronics; as a result, fully fold-in product **BN-[7]H** was obtained in 24% yield. The chemical structures of these NBN-doped benzo[*n*]helicenes (*n* = 5, 6, and 7) and *π*-extended helicenes were unambiguously verified by a combination of NMR spectrometry, high-resolution mass spectrometry, and single-crystal X-ray diffraction analysis (*vide infra*).

Structural Analysis

Single crystals of the racemic fold-in borylation products (**BN-[5]H**, **BN-[6]H**, and **BN-[7]H**) and pan-out borylation products (**E[6]H** and **E[4]H**) suitable for X-ray analysis were obtained by slow diffusion of methanol into toluene solutions at room temperature (Figure 3). The helicity was determined by summing the dihedral angles for the inner rim (φ). The φ values were 60.9°, 66.7°, and 97.9° for **BN-[5]H**, **BN-[6]H**, and **BN-[7]H** (Figure 3a), respectively, and these values increased along with the number of fused rings but were smaller than those of their corresponding carbo[*n*]helicenes (*n* = 5: φ = 67.9°;[57] *n* = 6: φ = 87.5°;[58] *n* = 7: φ = 109.3°.[59]). The B−C bond lengths in the N/B/N-phenalene cores were 1.502−1.551 Å, longer than common C = C bonds but comparable to those of C−C single bonds. However, as doubly bridged triarylboranes, the NBN-doped benzo[*n*]helicenes possessed much shorter C−B bond lengths than trimesitylborane (1.57−1.58 Å) with a propeller geometry. The angles of the boron atom and the adjacent two carbon atoms in the inner rims (∠C−B−C, 130.6°, 134.1°, and 131.7° for **BN-[5]H**, **BN-[6]H**, and **BN-[7]H**, respectively) were larger than their analogues in carbo[*n*]helicenes (∠C−C−C, 123−126°). As a result, the side arms of these NBN-helicenes were more stretched from each other than the carbo-analogs, contributing to lower barriers of racemization. The distortion was mainly determined by the numbers of *ortho*-fused 6-membered rings and the dihedral angle (θ) between the mean planes of the terminal rings. The resultant NBN-helicenes adopted highly distorted helical configurations with comparable θ values for their corresponding carbo[*n*]helicenes (Figure 3a), 44.7°, 54.4° and 35.0° for **BN-[5]H**, **BN-[6]H**, and **BN-[7]H**, respectively, and 47.3° (*n* = 5), 59.6° (*n* = 6), and 33.3° (*n* = 7) for carbo[*n*]helicenes. Furthermore, the 1,4-azaborine rings of **BN-[6]H** (rings C and D) had a nonplanarity value[60] of 0.118, which is larger than those of **BN-[5]H** (0.075 for ring C, and 0.094 for ring D) and **BN-[7]H** (0.080 for ring D, and 0.107 for ring E), revealing a more distorted ring confirmation of **BN-[6]H** (Table S10). The distance between terminal carbon atoms of the inner rim (d_{C1-C6}) for **BN-[5]H** was 3.13 Å (Figure 3a), and an obvious nuclear Overhauser effect (NOE) between protons at positions 1 and 6 was observed (Figure S40). The centroid-centroid distance of the overlapped benzene rings (A

https://doi.org/10.1021/prechem.3c00097
Precis. Chem. 2024, 2, 28−39

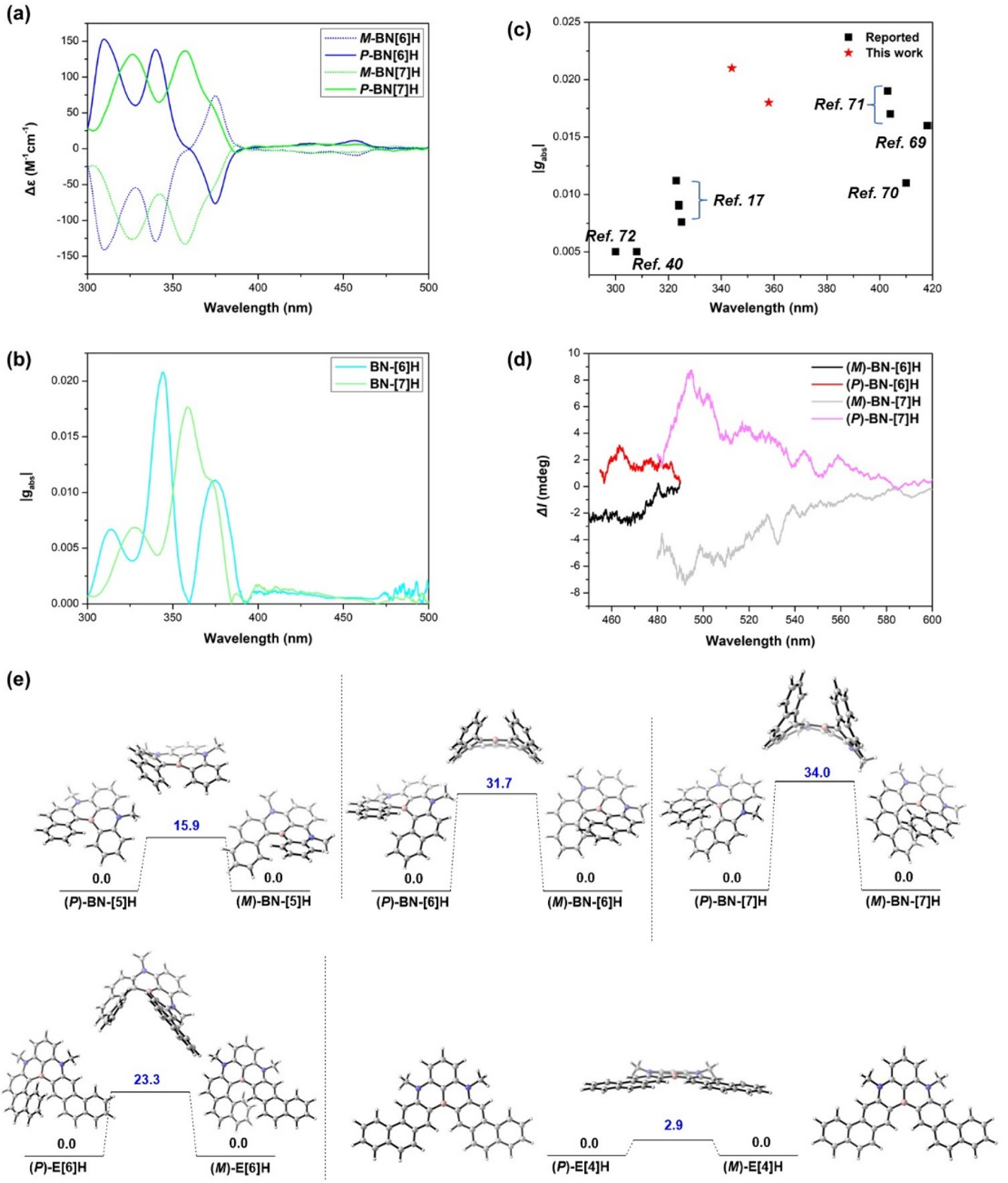

Figure 7. (a) ECD spectra of **BN**-[6]**H** and **BN**-[7]**H** in toluene. (b) $|g_{abs}|$ values of **BN**-[6]**H** and **BN**-[7]. (c) Comparison of $|g_{abs}|$ values with representative single-stranded helicenes. (d) CPL spectra of **BN**-[6]**H** and **BN**-[7]**H** in toluene. (e) Calculated interconversion process of NBN-doped helicenes at the B3LYP-D3BJ/Def2-TZVP (solvent toluene, PCM model) level. Relative Gibbs free energies are given in kcal mol^{-1}. *tert*-Butyl groups and the methyl group of the C ring in **BN**-[7]**H** are reduced to hydrogen atoms for simplicity.

and G) of **BN**-[7]**H** was determined to be 3.92 Å, which is slightly longer than that of carbo[7]helicene (3.83 Å), as a result of the longer B−C bonds. Notably, as the terminal rings of naphthalene moieties, the G ring of **BN**-[7]**H** was more shielded than the A rings of **BN**-[5]**H** and **BN**-[6]**H**, as indicated by the ^{1}H NMR spectra, which was ascribed to the significant overlap (Figures S1 and S2). **E**[6]**H** possessed the same number of *ortho*-fused rings as **BN**-[6]**H**, but the helicity of the former was

https://doi.org/10.1021/prechem.3c00097
Precis. Chem. 2024, 2, 28−39

slightly increased, as revealed by a larger φ value (75.3° vs 66.7°). As a π-extended benzo[4]helicene, **E[4]H** had the smallest φ value (33.4°) and θ value (θ_{CF} = 28.5°) among the five helicenes reported herein. The full pan-out orientation of phenanthrene moieties had a one-dimensional length of approximately 16 Å.

In the solid state, the unit cells of **BN-[5]H**, **BN-[7]H**, and **E[6]H** possessed four molecules with mirror symmetry in a stoichiometric ratio of 1:1, while **BN-[6]H** has six molecules in one cell unit. Interestingly, only (*P*)-enantiomers of **E[4]H** were found in the crystal, because of the very low racemization barrier, high flexibility, and strong intermolecular $\pi-\pi$ interactions. As depicted in Figure 3b, homochiral stacks of (*P*)- and (*M*)-enantiomers were observed in **BN-[5]H** and **BN-[7]H**, which arranged in a sandwich herringbone manner through intermolecular C−H···π interactions between molecules of the same configurations with distances of around 2.7 Å for **BN-[5]H**, 2.25 and 2.63 Å for **BN-[7]H**, respectively. **BN-[6]H** crystallized in a layered brickwork stacking manner without a deviation of ideal C_2-symmetry. A thread of alternative (*P*/*M*)-monomers was formed through strong $\pi-\pi$ interactions with an interplanar distance of 3.42 Å. Compared to **BN-[6]H**, slipped brickwork packing with alternating molecules of (*P*/*M*)-**E[6]H** was accommodated, accompanied by a much smaller void volume owing to stronger $\pi-\pi$ interactions. (*P*)-enantiomers of **E[4]H** were zipped into one-dimensional stacking with alternative orientations of *tert*-butyl groups filling the cavities of [4]helicene subunits.

Photophysical and Electrochemical Properties

The ultraviolet−visible (UV−vis) absorption spectra of **BN-[n]H** (*n* = 5−7), **E[6]H** and **E[4]H** in diluted toluene solutions were displayed in Figure 4a. The absorption peaks of the title compounds possess similar shapes with changes in wavelengths and intensities. **BN-[5]H** exhibited moderate absorption centered at 447 nm ($\varepsilon = 1.66 \times 10^4$ M^{-1} cm^{-1}) for the lowest energy transition with a shoulder band between 410 and 430 nm. The absorption peak of **BN-[6]H** was red-shifted to 456 nm ($\varepsilon = 1.71 \times 10^4$ M^{-1} cm^{-1}) with well-resolved vibronic progressions centered at 430 nm ($\varepsilon = 7.2 \times 10^3$ M^{-1} cm^{-1}). As elongated structures, **E[6]H** and **E[4]H** gave rise to further red-shifted absorption maxima (483 and 496 nm) with increased molar absorption coefficients (2.21×10^4 M^{-1} cm^{-1} and 2.51×10^4 M^{-1} cm^{-1}). Interestingly, **BN-[7]H** featuring asymmetric blades with significant overlap between terminal benzene rings has a distinct absorption band located at 400−500 nm. In stark contrast to **BN-[n]H** (n = 5, 6, and 7), the pristine carbo[*n*]helicene (n = 5−7) exhibited only weak hypochromically shifted absorption in the spectral range of 350−420 nm for the lowest-lying transition states.[61] Moreover, the absorption peaks of these NBN-doped helicenes were observed in the range 350−420 nm with moderate intensities and were ascribed to their higher transitions (mainly S2) according to the TD-DFT calculation at the PBE0/6-311G(d) level (Table S7). The lowest energy absorption bands corresponded predominantly to the HOMO → LUMO (the lowest unoccupied molecular orbitals) transitions (97−98%), with oscillator strengths (*f*) of 0.246 (**BN-[5]H**), 0.225 (**BN-[6]H**), 0.168 (**BN-[7]H**), 0.272 (**E[6]H**) and 0.402 (**E[4]H**).

Upon excitation, intense and sharp emission peaks were observed for diluted toluene solutions of NBN-doped helicenes (Figure 4b). The emission maxima (λ_{em}) were gradually bathochromically shifted from 461 to 467 and 494 nm for **BN-[5]H**, **BN-[6]H**, and **BN-[7]H**. When the fused ring number was increased to 9 for **E[6]H** and **E[4]H**, the emission peaks were further red-shifted to 507 and 516 nm, respectively, illustrating the capacity of tuning colors from blue to green by increased π-conjugation of these NBN-doped helicene emitters. Remarkably, the Stokes shifts (υ_a-υ_f) and fwhms of **BN-[5]H** (679 cm^{-1} and 25 nm), **BN-[6]H** (516 cm^{-1} and 23 nm), **BN-[7]H** (1496 cm^{-1} and 43 nm), **E[6]H** (980 cm^{-1} and 35 nm), and **E[4]H** (781 cm^{-1} and 28 nm) were relatively small, indicating the high rigidity of these distorted structures. Unlike the all-carbon analogues, such as, carbo[6]- and [7]-helicene, which gave rise to broad emission bands between 390 and 500 nm with Φ values of only around 4% and 2%,[12−17] respectively, NBN-doped helicenes in nondeoxygenated toluene yielded a narrowed peak pattern with impressive Φ values (37−55%). In contrast to doping with various atoms,[62−67] such as nitrogen,[62,63] oxygen,[64] silicon,[62,65] phosphorus[66] and sulfur,[62,67] nonbonded N/B/N-doping with multiple resonance effects[35] afforded heterohelicenes with narrow-band emission and further improved photoluminescence quantum yields.

To further evaluate the impact of NBN-doping on the photophysical and electrochemical properties, a computational study was conducted. The origin of the narrow emission bands was explained by the small structural changes between the ground states (S_0) and the lowest singlet states (S_1), which were confirmed by the extremely small root-mean-square deviation of the atomic positions (RMSD) (Figure 5a).[48] A significant correlation between the fwhm and RMSD was observed (Figure S11), while **BN-[6]H** yielded the narrowest fwhm and had the smallest RMSD value among these NBN-doped helicenes. The HOMOs and LUMOs were delocalized over the whole molecular skeleton (Figure 5b). Furthermore, the HOMOs and LUMOs were spatially well-separated, affording multi-resonant structures accompanied by minimized vibronic coupling and vibrational relaxation, which also explained the narrow emission bands.[35−38,68] The calculated HOMO−LUMO gaps ($\Delta E_{cal\text{-}H/L}$) were narrowed from 3.50 to 3.42 and 3.35 eV for **BN-[5]H**, **BN-[6]H**, and **BN-[7]H**, respectively. **E[6]H** and **E[4]H** have the same number of fused rings, and the calculated HOMO−LUMO gaps were further reduced to 3.22 and 3.15 eV, respectively. Interestingly, according to the nucleus independent chemical shifts (NICS) calculations, the slightly negative $NICS(1)_{zz}$ values of the 1,4-azaborine rings indicated the low aromatic character of these heterocycles, while the high aromaticity of other benzene rings was not substantially affected by NBN-doping or through space overlap (Table S10).

The fluorescence lifetimes (τ) were obtained by mono-exponential fitting of time-resolved photoluminescence (TRPL) decays, showing much lower values than those of carbohelicenes (6.5 5.3, 5.0, 6.0, and 5.1 ns for **BN-[5]H**, **BN-[6]H**, **BN-[7]H**, **E[6]H** and **E[4]H**, respectively) (Figure S12). The photophysical dynamics of these NBN-doped helicenes were further studied by femtosecond transient absorption (fs-TA) spectra with 267 nm excitation in dichloromethane solutions (Figures 6 and S13−S15). A very broad photoinduced absorption (PIA) signal was observed to emerge quite slowly (around 1 ps). The pump laser pulse had a much shorter time (120 fs), and this early rise in PIA was associated with internal conversion from the high-energy singlet state to the S_1 state accomplished by the structural relaxation of the molecules. Then (from 1 ps to ∼2 ns), an obviously gradual decrease in the broad band of 550−800 nm occurred, which was associated with the decay of singlet excitons. There was a relatively long-lived signal (>1−2 ns) with

https://doi.org/10.1021/prechem.3c00097
Precis. Chem. 2024, 2, 28−39

a PIA peak which decayed much slower than the broad band near the absorption edge for all samples. These were likely due to triplet excitons populated from intersystem crossing. These were dark triplets that eventually decay with nonradiative transition, as evident from the lack of delayed fluorescence or phosphorescence observed in TRPL measurements.

In addition, the cyclic voltammetry measurement revealed an oxidation wave from which the HOMO was deduced (Figure S16). The HOMO levels differed slightly from −5.41 to −5.43, −5.39, and −5.38 V for **BN-[5]H**, **BN-[6]H**, **BN-[7]H** and **E[6]H**, respectively. **E[4]H** has an irreversible oxidative peak with an onset of 0.63 eV. The optical and electrochemical parameters of these NBN-doped helicenes are summarized in Table 1.

Chiroptical Properties and Interconversion Process

The enantiomers of **BN-[6]H** and **BN-[7]H** were successfully resolved by HPLC on a chiral stationary phase (Figures S17 and S18). As shown in Figure 7a, their electronic circular dichroism (ECD) spectra recorded in a toluene solution adopted a perfect mirror-image pattern. The absolute configuration was assigned by comparing the experimental ECD spectra with the TD-DFT simulated spectra (Figure S19). Positive Cotton effects were observed in the ranges of 300−360 ($\Delta\varepsilon$ = +152 M^{-1} cm^{-1} at 310 nm, $\Delta\varepsilon$ = +138 M^{-1} cm^{-1} at 340 nm) and 390−470 nm, and negative Cotton effects were observed in the range of 360−390 nm ($\Delta\varepsilon$ = −77 M^{-1} cm^{-1} at 375 nm) for (*P*)-**BN-[6]H**. (*P*)-**BN-[7]H** also adopted similar patterns of Cotton effects; however, they differed in the wavelength ranges, which were slightly negative in the range of 380−395 nm ($\Delta\varepsilon$ = −5 M^{-1} cm^{-1} at 387 nm) (Figure 7a). The selective response of chiral molecules to left and right circularly polarized light was quantified by the absorption dissymmetry factor (g_{abs}) through the equation $g_{abs} = \Delta\varepsilon/\varepsilon$. Strong ECD bands were located at 344 nm for **BN-[6]H** and 358 nm for **BN-[7]H**, showing $|g_{abs}|_{max}$ values of 0.021 and 0.018, respectively (Figure 7b), which are among the highest $|g_{abs}|$ values of single-stranded helicenes in the UVA range (Figure 7c, Table S6).[17,40,69−72] Notably, carbo[6]-helicene featured a maximal g_{abs} value of 0.0105 in dichloromethane at 325 nm.[73] To understand the origin of the high g_{abs} values, TD-DFT calculations on the ground states for both two chiral BN-helicenes were performed at the PBE0/6-311G(d) level.[74,75] As summarized in Table S9, the maximal g_{abs} values were assigned to the $S_0 \rightarrow S_6$ transition for **BN-[6]H** and the $S_0 \rightarrow S_4$ transition for **BN-[7]H**. According to the theory, $g_{abs} = 4\cos\theta|m|/|\mu|$ and the high g_{abs} values in these two transitions are attributed to the significantly enhanced magnetic transition dipole moment (m) relative to that of other transitions. The g_{abs} values were almost minimal in the $S_0 \rightarrow S_1$ transition for both compounds because of the higher electric transition dipole moment (μ), lower m, and approaching 90° of these two vectors.

The circular polarized luminescence (CPL) spectra of enantiomeric pure samples of **BN-[6]H** and **BN-[7]H** were recorded in toluene (Figure 7d). The sign of the lowest-energy transition of ECD spectra of both compounds was identical with that of their CPL signal. The emission dissymmetry factor (g_{lum}) is one of the key parameters for assessing the performance of CPL-emitters. It was worth noting that **BN-[7]H** showed a boosted g_{lum} of 1.0×10^{-3} compared to that of **BN-[6]H** (g_{lum} = 0.4×10^{-3}) (Figure S21). It was reasonable that g_{lum} values were in the magnitude of 10^{-3} as the g_{abs} values of the $S_0 \rightarrow S_1$ transition were quite small.

The racemization barriers (relative Gibbs free energy) of the title NBN-doped helicenes (*tert*-butyl groups and the methyl group of the C ring in **BN-[7]H** were reduced to hydrogen atoms) were calculated at the B3LYP-D3BJ/Def2-TZVP (solvent toluene, PCM model) level (Figure 7e). As expected, the longer C−B bond lengths in the inner rims decreased the racemization barriers of **BN-[n]H** relative to the all carbon analogs.[76,77] According to the calculation, **BN-[5]H** was configurationally unstable, with a *P-M* interconversion barrier of 15.9 kcal mol^{-1}, which was significantly lower than that of carbo[5]helicene (24.4 kcal mol^{-1}). Although **BN-[6]H** and **BN7[H]** exhibited smaller energy barriers than their corresponding carbo[*n*]helicenes (n = 6 and 7), sufficient configurational stability for chiral resolution has been confirmed by chiral HPLC analysis. The interconversion barrier of **BN-[6]H** was determined to be 31.7 kcal mol^{-1}, which is smaller than that of carbo[6]helicene (36.9 kcal mol^{-1}). The interconversion behavior of **BN-[7]H** is depicted in Figure 7d, where only one transition state with C_1 symmetry was identified, with an energy barrier of 34.0 kcal mol^{-1}, which is much smaller than that of carbo[7]helicene (42.0 kcal mol^{-1}). Compared with **BN-[6]H**, **E[6]H** also consists of 6 rings in the helix backbone, and the much lower racemization barrier illustrates that the position of NBN-doping plays an important role in the conformational interconversion process. **E[4]H** has an almost planarized transition state with an energy barrier of only 2.9 kcal mol^{-1}, which complies with the requirements of the self-sorting arrangement in the solid state.

CONCLUSION

In summary, a family of NBN-doped benzo[n]helicenes (**BN-[n]H**, n = 5−7) and π-extended helicenes (**E[6]H** and **E[4]H**) was successfully achieved by fold-in/pan-out bora-Friedel−Crafts reaction, which presented in a scalable, modular, and programmable sequence. The inherently chiral nature of these heterohelicenes is unambiguously confirmed by the crystallographic characterizations and chiral HPLC resolutions. The incorporation of nonbonded boron and nitrogen atoms harnessed narrow-band emission and improved (chiral) optical properties to the novel single-stranded carbon helix for the first time. **BN-[6]H** manifests a highly twisted screw-like backbone with high configurational stability accompanied by strong circular dichroism (g_{abs} = 0.021), sharp emission peak (fwhm = 23 nm), and improved photoluminescence efficiency (Φ_{PL} = 55%). More importantly, the fold-in/pan-out selectivity of one-pot borylation in regard to the helix engineering in polycyclic conjugated hydrocarbon (PCH) by NBN-doping is anticipated to be applied in the fabrication of optoelectronic devices with fine-tuned chiroptical properties.

ASSOCIATED CONTENT

Data Availability Statement

CCDC 2235573, 2235575, 2235579, 2239651, and 2239653 contain the supplementary crystallographic data for this paper. These data can be obtained free of charge viawww.ccdc.cam.ac.uk/data_request/cif, or by emailing data_request@ccdc.cam.ac.uk, or by contacting The Cambridge Crystallographic Data-Centre, 12 Union Road, Cambridge CB2 1EZ, UK; fax: +441223 336033.

Supporting Information

The Supporting Information is available free of charge at https://pubs.acs.org/doi/10.1021/prechem.3c00097.

https://doi.org/10.1021/prechem.3c00097
Precis. Chem. 2024, 2, 28−39

Synthetic procedures and characterization data for new compounds, general experimental methods, DFT calculation details, and crystallographic data (PDF)
X-ray crystallographic data for **BN-[5]H** (CIF)
X-ray crystallographic data for **BN-[6]H** (CIF)
X-ray crystallographic data for **BN-[7]H** (CIF)
X-ray crystallographic data for **E[6]H** (CIF)
X-ray crystallographic data for **E[4]H** (CIF)

AUTHOR INFORMATION

Corresponding Authors

Zhaohui Wang − *Key Laboratory of Organic Optoelectronics and Molecular Engineering, Department of Chemistry, Tsinghua University, Beijing 100084, China;* orcid.org/0000-0001-5786-5660; Email: wangzhaohui@mail.tsinghua.edu.cn

Junzhi Liu − *State Key Laboratory of Synthetic Chemistry, HKU-CAS Joint Laboratory on New Materials and Department of Chemistry, The University of Hong Kong, Pokfulam, Hong Kong, China;* orcid.org/0000-0001-7146-0942; Email: juliu@hku.hk

Authors

Weiwen Zhuang − *State Key Laboratory of Synthetic Chemistry, HKU-CAS Joint Laboratory on New Materials and Department of Chemistry, The University of Hong Kong, Pokfulam, Hong Kong, China*

Yujian Liu − *Key Laboratory of Organic Optoelectronics and Molecular Engineering, Department of Chemistry, Tsinghua University, Beijing 100084, China*

Ziqi Deng − *State Key Laboratory of Synthetic Chemistry, HKU-CAS Joint Laboratory on New Materials and Department of Chemistry, The University of Hong Kong, Pokfulam, Hong Kong, China*

Yu Guo − *Department of Mechanical Engineering, The University of Hong Kong, Pokfulam, Hong Kong, China*

Philip C. Y. Chow − *Department of Mechanical Engineering, The University of Hong Kong, Pokfulam, Hong Kong, China;* orcid.org/0000-0002-2373-503X

David Lee Phillips − *State Key Laboratory of Synthetic Chemistry, HKU-CAS Joint Laboratory on New Materials and Department of Chemistry, The University of Hong Kong, Pokfulam, Hong Kong, China;* orcid.org/0000-0002-8606-8780

Wei Jiang − *Key Laboratory of Organic Optoelectronics and Molecular Engineering, Department of Chemistry, Tsinghua University, Beijing 100084, China;* orcid.org/0000-0002-0153-7796

Complete contact information is available at: https://pubs.acs.org/10.1021/prechem.3c00097

Author Contributions

†W.Z. and Y.L. contributed equally. All authors have given approval to the final version of the manuscript.

Notes

The authors declare no competing financial interest.

ACKNOWLEDGMENTS

This work was supported by the Hong Kong Research Grants Council (27301720, 17304021), National Natural Science Foundation of China (22122114, 22122503, 21790361). J.L. is grateful for the funding from The University of Hong Kong (HKU) and ITC to the SKL. We acknowledge the computer cluster (HPC2021) of HKU. We thank Prof. Yuan-Zhi Tan, Dr. Xiaohe Miao, Dr. Jianping Zhao for the single-crystal X-ray diffraction experiments and data analysis.

REFERENCES

(1) Shen, Y.; Chen, C.-F. Helicenes: synthesis and applications. *Chem. Rev.* **2012**, *112*, 1463−1535.
(2) Gingras, M. One hundred years of helicene chemistry. Part 1: non-stereoselective syntheses of carbohelicenes. *Chem. Soc. Rev.* **2013**, *42*, 968−1006.
(3) Gingras, M.; Félix, G.; Peresutti, R. One hundred years of helicene chemistry. Part 2: stereoselective syntheses and chiral separations of carbohelicenes. *Chem. Soc. Rev.* **2013**, *42*, 1007−1050.
(4) Gingras, M. One hundred years of helicene chemistry. Part 3: applications and properties of carbohelicenes. *Chem. Soc. Rev.* **2013**, *42*, 1051−1095.
(5) Dhbaibi, K.; Favereau, L.; Crassous, J. Enantioenriched helicenes and helicenoids containing main-group elements (B, Si, N, P). *Chem. Rev.* **2019**, *119*, 8846−8953.
(6) Meisenheimer, J.; Witte, K. Reduction von 2-nitronaphtalin. *Ber. Dtsch. Chem. Ges.* **1903**, *36*, 4153−4164.
(7) Hassey, R.; Swain, E. J.; Hammer, N. I.; Venkataraman, D.; Barnes, M. D. Probing the chiroptical response of a single molecule. *Science* **2006**, *314*, 1437−1439.
(8) Huang, Q.; Jiang, L.; Liang, W.; Gui, J.; Xu, D.; Wu, W.; Nakai, Y.; Nishijima, M.; Fukuhara, G.; Mori, T.; Inoue, Y.; Yang, C. Inherently chiral azonia[6]helicene-modified β-cyclodextrin: synthesis, characterization, and chirality sensing of underivatized amino acids in water. *J. Org. Chem.* **2016**, *81*, 3430−3434.
(9) Kiran, V.; Mathew, S. P.; Cohen, S. R.; Delgado, I. H.; Lacour, J.; Naaman, R. Helicenes-a new class of organic spin filter. *Adv. Mater.* **2016**, *28*, 1957−1962.
(10) Rodríguez, R.; Naranjo, C.; Kumar, A.; Matozzo, P.; Das, T. K.; Zhu, Q.; Vanthuyne, N.; Gómez, R.; Naaman, R.; Sánchez, L.; Crassous, J. Mutual monomer orientation to bias the supramolecular polymerization of [6]helicenes and the resulting circularly polarized light and spin filtering properties. *J. Am. Chem. Soc.* **2022**, *144*, 7709−7719.
(11) Feringa, B. L.; van Delden, R. A.; Koumura, N.; Geertsema, E. M. Chiroptical molecular switches. *Chem. Rev.* **2000**, *100*, 1789−1816.
(12) Vander Donckt, E.; Nasielski, J.; Greenleaf, J.R.; Birks, J.B. Fluorescence of the helicenes. *Chem. Phys. Lett.* **1968**, *2*, 409−410.
(13) Sapir, M.; Donckt, E. V. Intersystem crossing in the helicenes. *Chem. Phys. Lett.* **1975**, *36*, 108−110.
(14) Birks, J. B.; Birch, D. J. S.; Cordemans, E.; Donckt, E. V. Fluorescence of the higher helicenes. *Chem. Phys. Lett.* **1976**, *43*, 33−36.
(15) Nijegorodov, N. I.; Downey, W. S. The influence of planarity and rigidity on the absorption and fluorescence parameters and intersystem crossing rate constant in aromatic molecules. *J. Phys. Chem.* **1994**, *98*, 5639−5643.
(16) Kubo, H.; Hirose, T.; Matsuda, K. Control over the emission properties of [5]helicenes based on the symmetry and energy levels of their molecular orbitals. *Org. Lett.* **2017**, *19*, 1776−1779.
(17) Full, J.; Panchal, S. P.; Götz, J.; Krause, A. M.; Nowak-Król, A. Modular synthesis of organoboron helically chiral compounds: cutouts from extended helices. *Angew. Chem., Int. Ed.* **2021**, *60*, 4350−4357.
(18) Jakubec, M.; Storch, J. Recent advances in functionalizations of helicene backbone. *J. Org. Chem.* **2020**, *85*, 13415−13428.
(19) Saleh, N.; Shen, C.; Crassous, J. Helicene-based transition metal complexes: synthesis, properties and applications. *Chem. Sci.* **2014**, *5*, 3680−3694.
(20) Mori, K.; Murase, T.; Fujita, M. One-step synthesis of [16]helicene. *Angew. Chem., Int. Ed.* **2015**, *54*, 6847−6851.
(21) Bell, T. W.; Jousselin, H. Expanded heterohelicenes: molecular coils that form chiral complexes. *J. Am. Chem. Soc.* **1991**, *113*, 6283−6284.

(22) Kiel, G. R.; Patel, S. C.; Smith, P. W.; Levine, D. S.; Tilley, T. D. Expanded helicenes: a general synthetic strategy and remarkable supramolecular and solid-state behavior. *J. Am. Chem. Soc.* **2017**, *139*, 18456−18459.
(23) Oda, S.; Kawakami, B.; Yamasaki, Y.; Matsumoto, R.; Yoshioka, M.; Fukushima, D.; Nakatsuka, S.; Hatakeyama, T. One-shot synthesis of expanded heterohelicene exhibiting narrowband thermally activated delayed fluorescence. *J. Am. Chem. Soc.* **2022**, *144*, 106−112.
(24) Li, C.; Yang, Y.; Miao, Q. Recent progress in chemistry of multiple helicenes. *Chem.—Asian J.* **2018**, *13*, 884−894.
(25) Mori, T. Chiroptical properties of symmetric double, triple, and multiple helicenes. *Chem. Rev.* **2021**, *121*, 2373−2412.
(26) Jiang, W.; Wang, Z. Molecular carbon imides. *J. Am. Chem. Soc.* **2022**, *144*, 14976−14991.
(27) Fernández-García, J. M.; Evans, P. J.; Rivero, S. M.; Fernández, I.; García-Fresnadillo, D.; Perles, J.; Casado, J.; Martín, N. π-Extended corannulene-based nanographenes: selective formation of negative curvature. *J. Am. Chem. Soc.* **2018**, *140*, 17188−17196.
(28) Ma, J.; Fu, Y.; Dmitrieva, E.; Liu, F.; Komber, H.; Hennersdorf, F.; Popov, A. A.; Weigand, J. J.; Liu, J.; Feng, X. Helical nanographenes containing an azulene unit: synthesis, crystal structures, and properties. *Angew. Chem., Int. Ed.* **2020**, *59*, 5637−5642.
(29) Medel, M. A.; Tapia, R.; Blanco, V.; Miguel, D.; Morcillo, S. P.; Campaña, A. G. Octagon-embedded carbohelicene as a chiral motif for circularly polarized luminescence emission of saddle-helix nanographenes. *Angew. Chem., Int. Ed.* **2021**, *60*, 6094−6100.
(30) Reger, D.; Haines, P.; Amsharov, K. Y.; Schmidt, J. A.; Ullrich, T.; Bönisch, S.; Hampel, F.; Görling, A.; Nelson, J.; Jelfs, K. E.; Guldi, D. M.; Jux, N. A family of superhelicenes: easily tunable, chiral nanographenes by merging helicity with planar π systems. *Angew. Chem., Int. Ed.* **2021**, *60*, 18073−18081.
(31) Duan, C.; Zhang, J.; Xiang, J.; Yang, X.; Gao, X. Azulene-embedded [n]helicenes (n = 5, 6 and 7). *Angew. Chem., Int. Ed.* **2022**, *61*, No. e202201494.
(32) Campbell, P. G.; Marwitz, A. J. V.; Liu, S. Y. Recent advances in azaborine chemistry. *Angew. Chem., Int. Ed.* **2012**, *51*, 6074−6092.
(33) Stępień, M.; Gońka, E.; Żyła, M.; Sprutta, N. Heterocyclic nanographenes and other polycyclic heteroaromatic compounds: synthetic routes, properties, and applications. *Chem. Rev.* **2017**, *117*, 3479−3716.
(34) Borissov, A.; Maurya, Y. K.; Moshniaha, L.; Wong, W.; Żyła-Karwowska, M.; Stępień, M. Recent advances in heterocyclic nanographenes and other polycyclic heteroaromatic compounds. *Chem. Rev.* **2022**, *122*, 565−788.
(35) Hatakeyama, T.; Shiren, K.; Nakajima, K.; Nomura, S.; Nakatsuka, S.; Kinoshita, K.; Ni, J.; Ono, Y.; Ikuta, T. Ultrapure blue thermally activated delayed fluorescence molecules: efficient HOMO-LUMO separation by the multiple resonance effect. *Adv. Mater.* **2016**, *28*, 2777−2781.
(36) Oda, S.; Hatakeyama, T. Development of one-shot/one-pot borylation reactions toward organoboron-based materials. *Bull. Chem. Soc. Jpn.* **2021**, *94*, 950−960.
(37) Shin, I.; Lim, H. N.; Hong, W. P. 1,4-Azaborines: origin, modern synthesis, and applications as optoelectronic materials. *Synthesis* **2022**, *54*, 570−588.
(38) Chen, C.; Du, C.-Z.; Wang, X.-Y. The rise of 1,4-BN-heteroarenes: synthesis, properties, and applications. *Adv. Sci.* **2022**, *9*, No. 2200707.
(39) Hatakeyama, T.; Hashimoto, S.; Oba, T.; Nakamura, M. Azaboradibenzo[6]helicene: carrier inversion induced by helical homochirality. *J. Am. Chem. Soc.* **2012**, *134*, 19600−19603.
(40) Yuan, K.; Volland, D.; Kirschner, S.; Uzelac, M.; Nichol, G. S.; Nowak-Król, A.; Ingleson, M. J. Enhanced N-directed electrophilic C-H borylation generates BN-[5]- and [6]helicenes with improved photophysical properties. *Chem. Sci.* **2022**, *13*, 1136−1145.
(41) Shen, C. S.; Srebro-Hooper, M.; Jean, M.; Vanthuyne, N.; Toupet, L.; Williams, J. A. G.; Torres, A. R.; Riives, A. J.; Muller, G.; Autschbach, J.; Crassous, J. Synthesis and chiroptical properties of hexa-, octa-, and deca-azborahelicenes: influence of helicene size and of the number of boron atoms. *Chem.—Eur. J.* **2017**, *23*, 407−418.
(42) Full, F.; Wölflick, Q.; Radacki, K.; Braunschweig, H.; Nowak-Król, A. Enhanced optical properties of azaborole helicenes by lateral and helical extension. *Chem.—Eur. J.* **2022**, *28*, No. e202202280.
(43) Wu, X.; Huang, J.-W.; Su, B.-K.; Wang, S.; Yuan, L.; Zheng, W.-Q.; Zhang, H.; Zheng, Y.-X.; Zhu, W.; Chou, P.-T. Fabrication of circularly polarized MR-TADF emitters with asymmetrical peripheral-lock enhancing helical B/N-doped nanographenes. *Adv. Mater.* **2022**, *34*, No. 2105080.
(44) Zhang, Y.; Zhang, D.; Huang, T.; Gillett, A. J.; Liu, Y.; Hu, D.; Cui, L.; Bin, Z.; Li, G.; Wei, J.; Duan, L. Multi-resonance deep-red emitters with shallow potential-energy surfaces to surpass energy-gap law. *Angew. Chem., Int. Ed.* **2021**, *60*, 20498−20503.
(45) Li, J.-K.; Chen, X.-Y.; Guo, Y.-L.; Wang, X.-C.; Sue, A. C.-H.; Cao, X.-Y.; Wang, X.-Y. B,N-embedded double hetero[7]helicenes with strong chiroptical responses in the visible light region. *J. Am. Chem. Soc.* **2021**, *143*, 17958−17963.
(46) Yang, W.; Li, N.; Miao, J.; Zhan, L.; Gong, S.; Huang, Z.; Yang, C. Simple double hetero[5]helicenes realize highly efficient and narrowband circularly polarized organic light-emitting diodes. *CCS Chem.* **2022**, *4*, 3463−3471.
(47) Maeda, C.; Nagahata, K.; Shirakawa, T.; Ema, T. Azahelicene-fused BODIPY analogues showing circularly polarized luminescence. *Angew. Chem., Int. Ed.* **2020**, *59*, 7813−7817.
(48) Zhang, F.; Rauch, F.; Swain, A.; Marder, T. B.; Ravat, P. Efficient narrowband circularly polarized light emitters based on 1,4-B,N-embedded rigid donor-acceptor helicenes. *Angew. Chem., Int. Ed.* **2023**, *62*, No. e202218965.
(49) Hatakeyama, T.; Mizutani, A.; Koike, T. Organic electroluminescent element. U.S. Patent WO2017188111, November 2, 2017.
(50) Song, I.; Yoon, S.; Kim, S.; Park, S.-M.; Lee, T. W.; Jeong, J. H.; Yoo, J. Organic electroluminescent device. U.S. Patent US20200335705, October 22, 2020.
(51) Kim, C.; Shin, H. Organic light-emitting compound and organic electroluminescence element using same. U.S. Patent WO2022131768, June 23, 2022.
(52) Schickedanz, K.; Radtke, J.; Bolte, M.; Lerner, H.-W.; Wagner, M. Facile route to quadruply annulated borepins. *J. Am. Chem. Soc.* **2017**, *139*, 2842−2851.
(53) Ando, M.; Sakai, M.; Ando, N.; Hirai, M.; Yamaguchi, S. Planarized B,N-phenylated dibenzoazaborine with a carbazole substructure: electronic impact of the structural constraint. *Org. Biomol. Chem.* **2019**, *17*, 5500−5504.
(54) Narita, H.; Choi, H.; Ito, M.; Ando, N.; Ogi, S.; Yamaguchi, S. Fully fused boron-doped polycyclic aromatic hydrocarbons. *Chem. Sci.* **2022**, *13*, 1484−1491.
(55) Tanaka, T. Synthesis of novel heteronanographenes via fold-in approach. *Bull. Chem. Soc. Jpn.* **2022**, *95*, 602−610.
(56) Hirai, H.; Nakajima, K.; Nakatsuka, S.; Shiren, K.; Ni, J.; Nomura, S.; Ikuta, T.; Hatakeyama, T. One-step borylation of 1,3-diaryloxybenzenes towards efficient materials for organic light-emitting diodes. *Angew. Chem., Int. Ed.* **2015**, *54*, 13581−13585.
(57) Kuroda, R. Crystal and molecular structure of [5]helicene: crystal packing modes. *J. Chem. Soc. Perkin Trans. 2* **1982**, 789−794.
(58) Yoshida, Y.; Nakamura, Y.; Kishida, H.; Hayama, H.; Nakano, Y.; Yamochi, H.; Saito, G. Racemic charge-transfer complexes of a helical polycyclic aromatic hydrocarbon molecule. *CrystEngComm* **2017**, *19*, 3626−3632.
(59) Fuchter, M. J.; Weimar, M.; Yang, X.; Judge, D. K.; White, A. J. P. An unusual oxidative rearrangement of [7]-helicene. *Tetrahedron Lett.* **2012**, *53*, 1108−1111.
(60) Cheung, K. Y.; Xu, X.; Miao, Q. Aromatic saddles containing two heptagons. *J. Am. Chem. Soc.* **2015**, *137*, 3910−3914.
(61) Nakai, Y.; Mori, T.; Inoue, Y. Theoretical and experimental studies on circular dichroism of carbo[n]helicenes. *J. Phys. Chem. A* **2012**, *116*, 7372−7385.

(62) Uematsu, K.; Hayasaka, C.; Takase, K.; Noguchi, K.; Nakano, K. Transformation of thia[7]helicene to aza[7]helicenes and [7]helicene-like compounds via aromatic metamorphosis. *Molecules* **2022**, *27*, 606.
(63) Upadhyay, G. M.; Talele, H. R.; Bedekar, A. V. Synthesis and photophysical properties of aza[n]helicenes. *J. Org. Chem.* **2016**, *81*, 7751−7759.
(64) Shyam Sundar, M.; Bedekar, A. V. Synthesis and study of 7,12,17-trioxa[11]helicene. *Org. Lett.* **2015**, *17*, 5808−5811.
(65) Oyama, H.; Nakano, K.; Harada, T.; Kuroda, R.; Naito, M.; Nobusawa, K.; Nozaki, K. Facile synthetic route to highly luminescent sila[7]helicene. *Org. Lett.* **2013**, *15*, 2104−2107.
(66) Nakano, K.; Oyama, H.; Nishimura, Y.; Nakasako, S.; Nozaki, K. λ^5-Phospha[7]helicenes: synthesis, properties, and columnar aggregation with one-way chirality. *Angew. Chem., Int. Ed.* **2012**, *51*, 695−699.
(67) Licandro, E.; Cauteruccio, S.; Dova, D. Thiahelicenes: from basic knowledge to applications. *Adv. Heterocycl. Chem.* **2016**, *118*, 1−46.
(68) Qiu, X.; Tian, G.; Lin, C.; Pan, Y.; Ye, X.; Wang, B.; Ma, D.; Hu, D.; Luo, Y.; Ma, Y. Narrowband emission from organic fluorescent emitters with dominant low-frequency vibronic coupling. *Adv. Opt. Mater.* **2021**, *9*, No. 2001845.
(69) Kubo, H.; Hirose, T.; Nakashima, T.; Kawai, T.; Hasegawa, J. Y.; Matsuda, K. Tuning transition electric and magnetic dipole moments: [7]helicenes showing intense circularly polarized luminescence. *J. Phys. Chem. Lett.* **2021**, *12*, 686−695.
(70) Saal, F.; Zhang, F.; Holzapfel, M.; Stolte, M.; Michail, E.; Moos, M.; Schmiedel, A.; Krause, A. M.; Lambert, C.; Würthner, F.; Ravat, P. [n]Helicene diimides (n= 5, 6, and 7): through-bond *versus* through-space conjugation. *J. Am. Chem. Soc.* **2020**, *142*, 21298−21303.
(71) Yanagi, T.; Tanaka, T.; Yorimitsu, H. Asymmetric systematic synthesis, structures, and (chir)optical properties of a series of dihetero [8]helicenes. *Chem. Sci.* **2021**, *12*, 2784−2793.
(72) Yamamoto, Y.; Sakai, H.; Yuasa, J.; Araki, Y.; Wada, T.; Sakanoue, T.; Takenobu, T.; Kawai, T.; Hasobe, T. *J. Phys. Chem. C* **2016**, *120*, 7421−7427.
(73) Tanaka, H.; Ikenosako, M.; Kato, Y.; Fujiki, M.; Inoue, Y.; Mori, T. Symmetry-based rational design for boosting chiroptical responses. *Commun. Chem.* **2018**, *1*, 38.
(74) Liu, Y.; Ma, Z.; Wang, Z.; Jiang, W. Boosting circularly polarized luminescence performance by a double π-helix and heteroannulation. *J. Am. Chem. Soc.* **2022**, *144*, 11397−11404.
(75) Lu, T.; Chen, F. Multiwfn: a multifunctional wavefunction analyzer. *J. Comput. Chem.* **2012**, *33*, 580−592.
(76) Barroso, J.; Cabellos, J. L.; Pan, S.; Murillo, F.; Zarate, X.; Fernandez-Herrera, M. A.; Merino, G. Revisiting the racemization mechanism of helicenes. *Chem. Commun.* **2018**, *54*, 188−191.
(77) Ravat, P. Carbo[n]helicenes restricted to enantiomerize: an insight into the design process of configurationally stable functional chiral PAHs. *Chem.—Eur. J.* **2021**, *27*, 3957−3967.

https://doi.org/10.1021/prechem.3c00097
Precis. Chem. 2024, 2, 28−39